JBC RESEARCH ARTICLE

Coevolution of the bacterial pheromone ComS and sensor ComR fine-tunes natural transformation in streptococci

Received for publication, July 27, 2021, and in revised form, October 17, 2021 Published, Papers in Press, October 27, 2021,
https://doi.org/10.1016/j.jbc.2021.101346

Laura Ledesma-García[1,*], Imke Ensinck[1], Denis Dereinne[1], Felipe Viela[1], Johann Mignolet[1], Yves F. Dufrêne[1], Patrice Soumillion[1], Sylvie Nessler[2], and Pascal Hols[1,*]

From the [1]Louvain Institute of Biomolecular Science and Technology (LIBST), Université catholique de Louvain, Louvain-La-Neuve, Belgium; [2]CEA, CNRS, Institute for Integrative Biology of the Cell (I2BC), Université Paris-Saclay, Gif-sur-Yvette, France

Edited by Chris Whitfield

Competence for natural transformation extensively contributes to genome evolution and the rapid adaptability of bacteria dwelling in challenging environments. In most streptococci, this process is tightly controlled by the ComRS signaling system, which is activated through the direct interaction between the (R)RNPP-type ComR sensor and XIP pheromone (mature ComS). The overall mechanism of activation and the basis of pheromone selectivity have been previously reported in Gram-positive salivarius streptococci; however, detailed 3D-remodeling of ComR leading up to its activation remains only partially understood. Here, we identified using a semirational mutagenesis approach two residues in the pheromone XIP that bolster ComR sensor activation by interacting with two aromatic residues of its XIP-binding pocket. Random and targeted mutagenesis of ComR revealed that the interplay between these four residues remodels a network of aromatic–aromatic interactions involved in relaxing the sequestration of the DNA-binding domain. Based on these data, we propose a comprehensive model for ComR activation based on two major conformational changes of the XIP-binding domain. Notably, the stimulation of this newly identified trigger point by a single XIP substitution resulted in higher competence and enhanced transformability, suggesting that pheromone-sensor coevolution counter-selects for hyperactive systems in order to maintain a trade-off between competence and bacterial fitness. Overall, this study sheds new light on the ComRS activation mechanism and how it could be exploited for biotechnological and biomedical purposes.

Bacteria have developed diverse horizontal gene transfer mechanisms that favor their adaptation and survival to a fluctuating and competitive ecological niche (1). Among those, natural DNA transformation allows the acquisition of new genetic traits from phylogenetically close and distant species (2–4). Regarding pathogenic bacteria, this increase in genome plasticity has been linked to the gain of virulence-related mechanisms and multidrug resistance, improving their success during host infection (2, 5).

During the natural transformation process, bacteria must enter a transitory physiological state called competence (3, 6), where a master transcriptional regulator triggers the expression of the genes encoding the transformasome (7). This multiprotein machinery captures, translocates, and finally integrates extracellular DNA fragments into the genome of competent bacteria (7). Competence is an energy-consuming process that results in fitness burden and affects cell division and chromosome integrity (8, 9). Hence, bacteria have orchestrated complex regulatory mechanisms to minimize the activation time window and avoid its fortuitous upregulation under inappropriate environmental conditions (10–12).

In streptococci, regulation of competence is primarily performed by the alternative sigma factor ComX (also called SigX, σ^X) that transiently associates with the RNA polymerase to induce transcriptional reprogramming (13, 14). Besides, the proximal transcriptional control of this master regulator is executed by a cell-to-cell communication system based on short linear peptide pheromones (13). Two exclusive systems (*i.e.*, ComCDE or ComRS) trigger ComX production and ensure a robust competence activation through the boost of signaling peptide production (positive feedback loop) above a specific pheromone concentration threshold (13). Species of the mitis and anginosus groups use the Competence-Stimulating Peptide (CSP, mature form of the precursor ComC) to extracellularly stimulate the transmembrane histidine kinase ComD that autophosphorylates and subsequently activates the response regulator ComE, *via* a phosphorelay event (15–17). In contrast, in the salivarius, pyogenic, bovis, and suis groups, the SigX-Inducing Peptide (XIP, mature form of the precursor ComS) exported by producer cells is reimported into the intracellular space of responder cells to bind and activate the cytoplasmic transcriptional regulator ComR (Fig. 1*A*) (13, 18–22). Thus, the phosphorylated ComE or the complex ComR·XIP will bind specific promoter sequences to activate transcription of the competence regulon, including *comX* and their cognate pheromone-encoding gene (Fig. 1*A*) (13).

ComR belongs to the (R)RNPP (for the original members (Rgg,) Rap, NprR, PlcR, and PrgX) superfamily of transcriptional regulators ubiquitous in Firmicutes (23). Several crystal structures of (R)RNPPs have been solved, demonstrating that they canonically exhibit an all-α two-domain structure formed

* For correspondence: Pascal Hols, Pascal.Hols@uclouvain.be; Laura Ledesma-García, Laura.Ledesma@uclouvain.be.

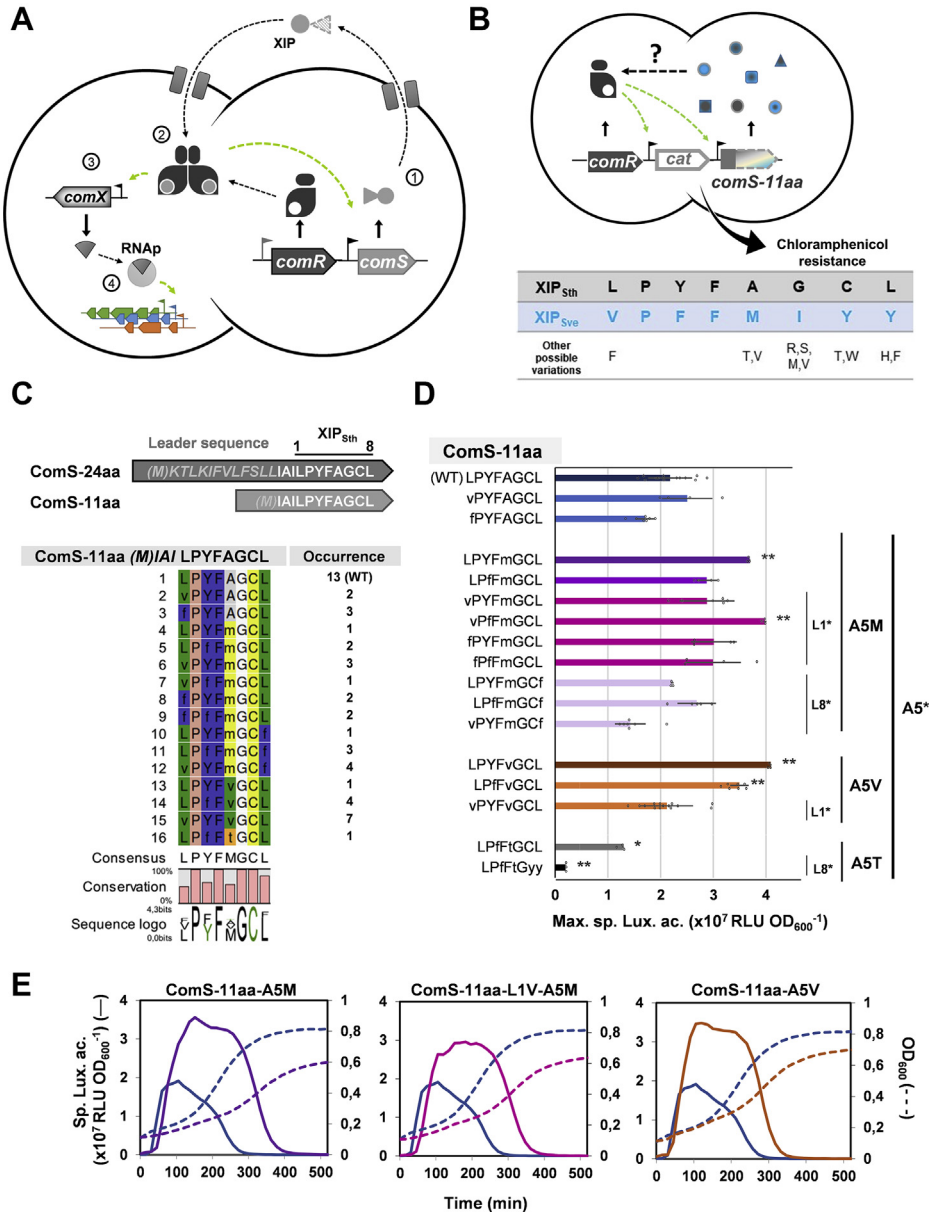

Figure 1. XIP semirational mutagenesis. *A*, ComRS system in streptococci. The ComS precursor is exported and matured into the extracellular XIP peptide (1), (re)imported by an oligopeptide transporter for its interaction with the ComR sensor, triggering its dimerization (2). The resulting ComR·XIP complex activates *comS*, (positive feed-back loop) and *comX* (master regulator) (3). ComX (σ^X) binds RNA-polymerase (RNAp) inducing competence transcriptional reprogramming (4). *B*, screening strategy for XIP mutagenesis. A library of semirandomized *comS-11aa* (*blue-gray arrow*, C-terminal 8 aa) under the control of the competence-inducible promoter (P_{comS}) is expressed into a *S. thermophilus* reporter strain carrying a chloramphenicol resistance gene (*cat*) fused to P_{comS}. ComR-activating peptides trigger their own production and chloramphenicol resistance. Residues corresponding to XIP_{Sth} (*gray*) and XIP_{Sve} (*blue*) were allowed in the degenerate oligonucleotide used for building the genetic library. Other possible residues at each XIP position are indicated below. *C*, sequence alignment of $ComR_{Sth}$-activating peptide variants. The sequences of the full-length precursor (ComS-24aa, leader sequence in *gray*), the native extracellular XIP peptide (ComS-11aa, shown in *white*), and the minimal interacting XIP peptide (XIP_{Sth}, 8 aa at C-terminus) of *S. thermophilus* are indicated on the *top* of the alignment. The occurrence of each peptide variant among 51 selected clones is indicated on the *right*. Residues are color-coded according to the Rasmol color scheme (53) and the consensus sequence is shown underneath. The Bits represent the relative frequency of residues. *D*, maximum specific luciferase activity (RLU OD_{600}^{-1}) of cytoplasmically expressed peptide variants. Activation by ComS-11aa (M)IAILPYFAGCL (positive control), (M)IAILPfFtGyy variant (negative control) or other peptide variants was monitored from a strain carrying a P_{comS}-*luxAB* fusion. Peptide variants carrying methionine, valine, or threonine substitutions at XIP position 5 are colored in *purple*, *orange*, or *gray* spectra, respectively. * indicates a mutation at residue L1, A5, or L8. Experimental values are mean ± SD of at least three independent replicates. Significant differences (ComS-11aa WT as reference) calculated by Student unpaired *t* test are indicated (**p-value < 0.01, *p-value < 0.05). *E*, kinetics of luciferase activation (*solid lines*) and growth curves (*dotted lines*) of reporter strains producing peptide variants ComS-11aa-A5M (*purple*), ComS-11aa-L1V-A5M (*fuchsia*), or ComS-11aa-A5V (*orange*). The control ComS-11aa WT (*blue*) is represented in all graphs. One representative experiment of three independent experiments showing similar results.

by a N-terminal helix-turn-helix (HTH) DNA-binding domain and a C-terminal tetratricopeptide repeat (TPR)-type peptide-binding domain (23–28). In the case of ComR, the HTH-domain is composed of five α-helices while the TPR-domain encompasses five pairs of anti-parallel α-helices (forming 5 TPR-subdomains) and a single C-terminal CAP

helix (capping helix α16) (27, 29). These detailed structure–function studies revealed that all (R)RNPPs undergo various conformational changes upon pheromone interaction that result in very diverse regulatory mechanisms (24, 26). In contrast to other members of the family, ComR is monomeric in the absence of peptide and only adopts its active dimeric form in the presence of XIP (29, 30). While apo-ComR displays a sequestered HTH domain fastened by the TPR domain, XIP binding induces conformational changes resulting in dimerization of the TPR domain and allosteric release of the two DNA-binding domains (29, 30). This idiosyncratic molecular mechanism ensures locking of the transcriptional regulator in the absence of its specific inducing pheromone.

Phylogenetic studies suggested a pheromone-sensor coevolution, which leads to primary sequence divergences among ComRS systems, often resulting in the absence of cross talk between streptococcal species (19, 27). Structural comparison between ComR·XIP complexes from two species of the salivarius group that do not cross talk, *Streptococcus thermophilus* and *Streptococcus vestibularis*, showed a conserved XIP-binding mode and helped pinpointing the minimal key residues in ComR and XIP required for peptide selectivity (30). These studies also allowed us to refine the activation model of the ComRS system. Main pillars of the TPR conformational change triggering dimerization and release of the HTH domain were highlighted. In particular, we showed the essential role of the XIP-induced reorientation of the TPR-1 (α6 and α7 helices) and TPR-2 (α8 and α9 helices) subdomains and recruitment of the CAP helix. In addition, these studies also suggested that additional interactions, such as those observed between two ComR aromatic residues and the hydrophobic residue at XIP N-terminus, could also play a major role in the activation mechanism and peptide selectivity (29, 30).

In this work, we use accelerated evolution of XIP pheromones from two orthologous systems to shed light on novel aspects of ComRS evolution and activation mechanism. Notably, a single pheromone mutation that increases ComR-XIP hydrophobic contacts drastically enhances DNA transformation, suggesting that evolution has kept this process under strict control to minimize fitness costs. A detailed reciprocal investigation of ComR-XIP interacting residues revealed an underestimated critical step of the ComRS activation mechanism.

Results

Exploring the landscape of active peptides between salivarius streptococci pheromones

In order to identify peptide variants that could foster ComR activation in *S. thermophilus*, an *in vivo* method based on their positive screening in selective medium was designed by fusing a ComR-responsive promoter (*comS* promoter [P_{comS}] as proxy) to a gene conferring resistance to chloramphenicol (P_{comS}-*cat*). Then, we generated a small semirational peptide library by using degenerate primers allowing all residue combinations between XIP_{Sth} ($L_1PYFAGCL_8$) from *S. thermophilus* and XIP_{Sve} ($V_1PFFMIYY_8$) from *S. vestibularis* (Fig. 1*B*) (30). Due to the degenerate nature of the genetic code, residues not present in XIP_{Sth} and XIP_{Sve} sequences were possible at some positions (Fig. 1*B*), resulting in a predicted library of 2304 peptide variants. To minimize interferences with degradation and translocation processes, we chose to express peptide variants with three additional N-terminal residues corresponding to the native extracellular peptide ($ComS_{\Delta 2-13}$, 11 aa) (20). These peptides are unable to be exported in the spontaneously transformable strain *S. thermophilus* LMD-9. The system was validated for competence activation using a luminescence reporter strain (P_{comS}-*luxAB*) (Fig. S1*A*).

A total of 51 candidates were identified on chloramphenicol plates with the most prevalent peptide (13 instances) corresponding to wild-type XIP_{Sth}. The alignment of 15 nonredundant peptide variants with the reference sequence (Fig. 1*C*) showed that most of the permissive positions (four out of six) could be mutated. The absence of variations at two positions, XIP_{Sth} G6 and C7, strikingly suggests that their modifications can drastically affect peptide·ComR complex formation/activation. XIP_{Sth} position 3 was occupied by either a tyrosine (∼60% of peptide variants) or a phenylalanine (∼40%), supporting previous results that a substitution at this position by an alternative aromatic amino acid is tolerated without major effect (19). Interestingly, ∼20% of peptide variants showed that XIP_{Sth} L8, of which carboxylate group was reported as critical for ComR binding (29, 30), could be replaced by the aromatic residue phenylalanine when present with the additional A5M mutation. Finally, XIP_{Sth} L1 and A5 showed the highest permissiveness by displaying all allowed modifications. Substitutions at those two positions are found in 50% and ∼80% of peptide variants, respectively. The permissiveness of these two XIP positions correlates with natural variations observed in XIPs from salivarius streptococci, as XIP-1 and XIP-5 can be substituted by L, V, A, C and A, T, M, I, respectively (30).

Altogether, this semirational mutagenesis supports the high permissiveness of $ComR_{Sth}$ for its activation by a range of XIP variants (30). However, the observed tolerability at each XIP position is strikingly variable: from strict (*i.e.*, XIP-6 and XIP-7) to highly permissive (*i.e.*, XIP-1 and XIP-5) with a predominant tolerance at XIP position 5.

Cytoplasmic production of XIP-5 variants improves $ComR_{Sth}$ activation

The capacity of the peptide variants for transcriptional activation was measured by luminescence assays (P_{comS} as proxy) and compared with the strain producing $ComS_{Sth}$-11 aa (positive control) (Fig. 1*D*). A potential candidate (LPFFTGYY at C-terminus) that was unable to grow on selective medium was also incorporated as negative control (Figs. 1*D* and S1*B*).

Peptide variants carrying a single modification in L1 (L1V or L1F) were not significantly altered in their activation capacity while those harboring A5M or A5V increased up to twice the signal compared with the wild-type sequence. Moreover, strains carrying those last two modifications displayed an

extended activation accompanied by a slight decrease of growth as expected for a higher competence triggering (Fig. 1*E*) (18, 31). In most cases, the association of A5M or A5V with single or multiple L1/Y3/L8 modifications reduced the activation capacity (Fig. 1*D*). The most severe reduction included a combination of A5M with L8F, supporting previous data on the importance of a branched-chain amino acid at XIP-8 for optimal ComR activation (19).

This expression analysis suggests that modifications at XIP position 5 (*i.e.*, A5M or A5V) boosts ComR activation and may indicate that the native XIP_{Sth} is not the most active pheromone variant.

Exogenous supply and native production of XIP-A5M increase competence

In order to confirm the data obtained from the screening, the last 8 aa of two more active peptides (*i.e.*, XIP-A5M and XIP-L1V-A5M) were chemically synthetized. These peptide variants were selected in order to study the effect of the A5M variation alone or in combination with a modification at XIP position 1. Luminescence assays with increasing extracellular concentrations of those peptides were performed using a reporter strain (P_{comS} as proxy) lacking the *comS* gene (Fig. 2*A*). In agreement with screening data, addition of XIP-A5M and XIP-L1V-A5M resulted in a similar increased and extended transcriptional activation with an approximately fourfold lower EC_{50} than wild-type XIP_{Sth} (Fig. 2, *A* and *B*). As expected for a strong competence activation, the addition of these two peptides had a negative effect on the growth rate of the reporter strain (Fig. 2*B*).

To investigate more deeply the role of substitutions at XIP position 5, we compared the impact of variations identified during the screen (*i.e.*, A5M, A5V, and A5T) or observed in some natural XIPs from salivarius streptococci (*i.e.*, A5T and A5I) (13, 30). The titration of the synthetic XIP_{Sth} variants showed that the A5T substitution is neutral while all the others are promoting activation (Fig. 2*C*). Considering the tested peptides, these results highlight a positive correlation between hydrophobicity (and bulkiness/length) of the side chain of XIP-5 residue and its ability to improve activation (A5M > A5I > A5V > A5T/A5). They also show that a methionine at that position is the most efficient to boost activation (Fig. 2*C*).

Finally, we evaluated if the genome-encoded version of XIP-A5M or and XIP-L1V-A5M as full-length precursor

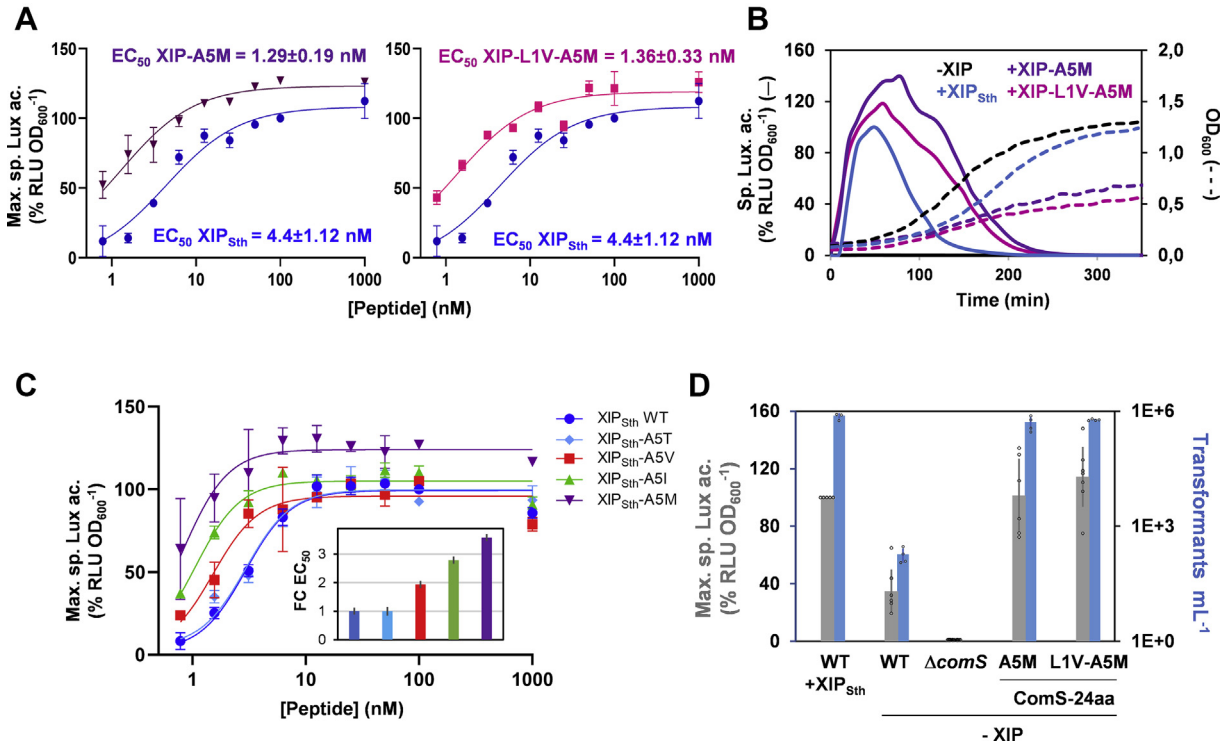

Figure 2. *In vivo* effect of synthetic pheromone variants. *A*, dose response of P_{comS} activity upon addition of synthetic (8 aa) XIP_{Sth} WT (*blue*), XIP-A5M (*purple*), or XIP-L1V-A5M (*fuchsia*). Maximum specific luciferase activity (% RLU × OD_{600}^{-1}) was monitored by using a *S. thermophilus* Δ*comS* reporter strain (P_{comS}-*luxAB*). The value obtained in the presence of 100 nM XIP_{Sth} was used as reference. Plots were fitted with the Hill equation to calculate the EC_{50} values that are indicated in the graphs. *B*, kinetics of luciferase activation (*solid lines*) and growth curves (*dotted lines*) of the reporter strain upon addition (100 nM) of synthetic XIP_{Sth} WT (*blue*), XIP-A5M (*purple*), or XIP-L1V-A5M (*fuchsia*), or in absence of peptide (*black*). *C*, dose response of P_{comS} activity upon addition of synthetic XIP_{Sth} WT (*blue*), or XIP-5 variants: XIP-A5T (*light blue*), XIP-A5V (*red*), XIP-A5I (*green*), or XIP-A5M (*purple*). The monitoring of luciferase activity and estimation of EC_{50} were performed as in panel *A*. The *inset* represents the fold change (FC) in EC_{50} of each XIP-5 variant using as reference the EC_{50} of XIP_{Sth} WT. Increase in fold change is representative of a decrease in EC_{50} compared with XIP_{Sth} WT fixed at 1. *D*, maximum specific luciferase activity (% RLU × OD_{600}^{-1}; *gray bars*) and transformation efficiency (transformants × ml^{-1}; *blue bars*) of *S. thermophilus* reporter strains producing the full-length precursor ComS-24aa WT, ComS-24aa-A5M or ComS-24aa-L1V-A5M. *S. thermophilus* WT in the presence of 100 nM XIP_{Sth} and a Δ*comS* mutant strain were included as positive and negative control, respectively. The WT strain in the presence of XIP_{Sth} is used as reference to normalize the maximum specific luciferase activity. In *A*, *C*, and *D*, experimental values represent the mean ± SD of at least three independent replicates.

(24 aa) could be able to spontaneously activate DNA transformation. Reporter strains harboring the full-length *comS* gene encoding the peptide variants were constructed by site-directed mutagenesis. Then, their capacity for transcriptional activation (P_{comS} as proxy) and spontaneous transformation were measured (Fig. 2*D*). A direct correlation between an enhanced competence gene expression and an increased transformation yield was confirmed for the native expression of XIP-A5M and XIP-L1V-A5M. Remarkably, the transformation rate of these two mutants was ∼3000-fold higher than the wild-type strain and similar to the addition of extracellular wild-type XIP_{Sth}. These results contrast with previous results showing that transformation efficiency was much lower with natively produced XIP than with synthetic XIP added to the extracellular medium (18).

Altogether, these experiments are conclusively highlighting the mild to strong improvement of competence activation and natural transformation generated by the A5M modified peptide.

XIP-A5M binds strongly and with a higher affinity to ComR

In order to shed light on the mechanism behind the improvement of competence activation produced by the XIP-A5M variant, different *in vitro* tests were performed to study its binding capacity to $ComR_{Sth}$.

As a first approach, its direct interaction with ComR was analyzed by fluorescent polarization (FP) assays as previously described (30, 32). For this purpose, a fixed amount of fluorophore-conjugated XIP_{Sth} WT or XIP-A5M was titrated with increasing concentrations of purified $ComR_{Sth}$. Anisotropy measurements revealed that the EC_{50} value for XIP-A5M was twice lower than XIP_{Sth}, demonstrating a higher affinity for the peptide variant (Fig. 3*A*). Moreover, competition assays were performed to test the ability of unlabeled ligands (XIP_{Sth}

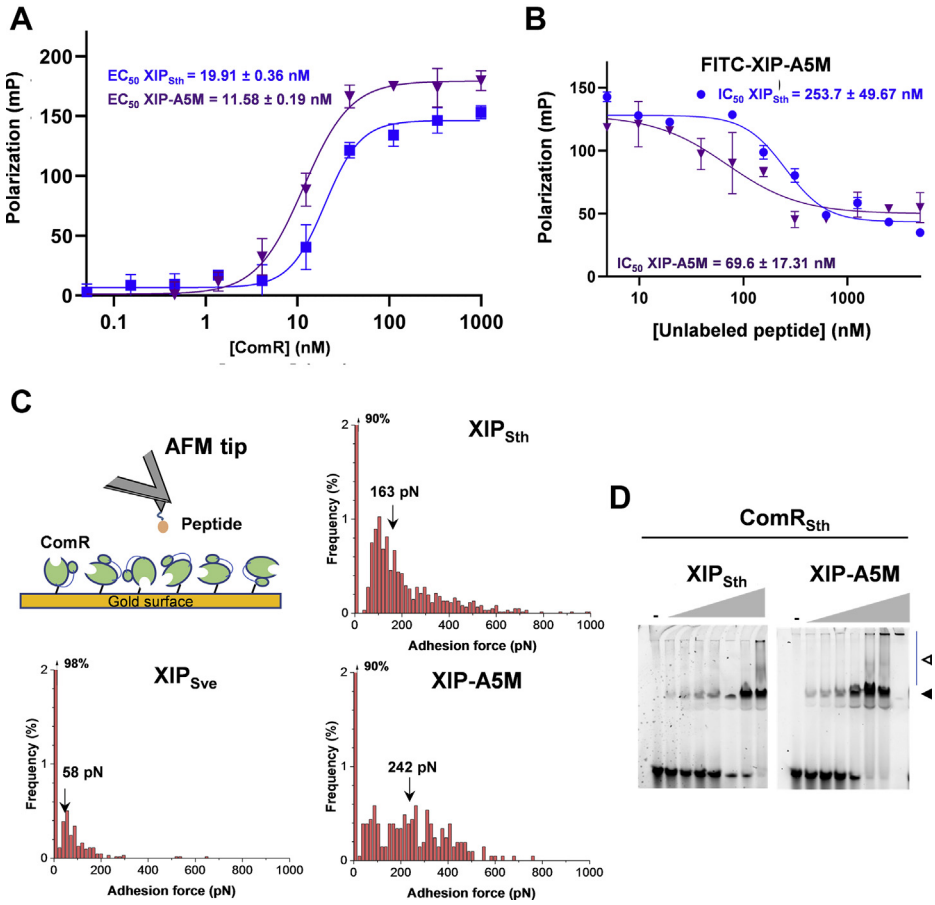

Figure 3. *In vitro* measurements of ComR-XIP interaction. *A*, fluorescence polarization assays. Titration was performed in the presence of a fixed concentration of FITC N-labeled XIP_{Sth} or FITC N-labeled XIP-A5M peptide (30 nM; *blue* or *purple*, respectively) and serial dilutions of ComR starting from 1 μM. Experimental values represent the mean ± SD of at least three independent replicates. Curves were fitted with the Hill equation to calculate the EC_{50} values. *B*, competition assay. Measure of decrease of fluorescent polarization signal upon addition of increasing concentrations of the unlabeled peptides XIP_{Sth} (*blue*) or XIP-A5M (*purple*) (from 0 to 5 μM) in the presence of a fixed concentration of FITC N-labeled XIP-A5M peptide (30 nM) and of $ComR_{Sth}$ (250 nM). Experimental values represent the mean ± SD of two independent replicates. Curves were fitted to calculate IC_{50} values. *C*, atomic force spectroscopy assay. Schematic representation of AFM setup for single molecule force spectroscopy experiments where $ComR_{Sth}$ is attached to the gold-coated glass coverslip and the XIP peptide to the cantilever. Binding force histogram of the interaction between $ComR_{Sth}$ and XIP_{Sth} WT, XIP_{Sve}, or XIP-A5M peptides. The median value (pN) is indicated in each histogram. Around 1000 curves were acquired per surface assayed from three biological replicates of each experiment where three surfaces were analyzed. *D*, electrophoretic mobility shift assay. Labeled P_{comS} 40-bp DNA fragments (20 ng) were incubated with a fixed concentration of $ComR_{Sth}$ WT (1 μM) in the absence of peptide (–) or in the presence of increasing concentrations of peptide XIP_{Sth} or the variant XIP-A5M (from 0 to 2 μM).

or XIP-A5M) to compete with the labeled form of FITC-XIP-A5M for ComR binding. The results showed a threefold lower IC_{50} value for unlabeled XIP-A5M than for the wild-type peptide, confirming the higher affinity of the modified peptide (Fig. 3*B*). As a second approach, the interaction between ComR and different peptides was probed by single molecule force spectroscopy using atomic force microscopy (AFM) (Fig. 3*C*). For this technique, the different peptides containing a 7-aa flexible linker (poly-Gly) at their N-terminus were grafted on the AFM tip, while $ComR_{Sth}$ was attached on the surface of a gold-coated coverslip. Unlike the noncognate XIP_{Sve} that showed low binding frequency (∼2%) and weak interaction force (range from 20 to 200 pN; median value of 58 pN), XIP_{Sth} showed a broad distribution of binding forces ranging from 60 to 1000 pN with a median value of 163 pN and a binding probability of ∼10% (Fig. 3*C*). After injection of soluble XIP_{Sth}, we observed a significant drop of the binding frequency to 3% (Fig. S2) that demonstrates the specificity of the $ComR_{Sth}$-XIP_{Sth} interaction. The XIP-A5M peptide produced a binding probability of 10% comparable to the wild-type XIP_{Sth}. As observed for XIP_{Sth}, XIP-A5M also exhibited a broad distribution of the binding force (ranging from 60 to 780 pN); however, XIP-A5M shifted the frequency distribution from low to high binding force (median value of 242 pN) (Fig. 3*C*), suggesting a stronger interaction with ComR. In line with the above results, electrophoretic mobility shift assays showed that XIP-A5M improved the binding of $ComR_{Sth}$ to P_{comS}, complexing the total amount of probe at lower peptide concentrations compared with XIP_{Sth} (Fig. 3*D*).

Thus, the A5M substitution improves XIP interaction in the ComR binding pocket, resulting in a more efficient formation of the ComR·XIP complex.

XIP-1/5 interacting residues F171–F174 are synergistically activating ComR

In parallel to XIP mutagenesis, we performed a random mutagenesis of $ComR_{Sth}$ using a similar screening strategy in a ComS-deficient strain with the aim to obtain mutants being natively constitutive (Fig. S3*A*). Those mutants deserve a special interest since the mutated position(s) could correspond to critical control point(s) in the ComR activating mechanism such as reported before for the release of the HTH-domain (29). We identified ∼30 mutants that showed an increased level of constitutive activation that was enhanced by the extracellular addition of the cognate peptide XIP_{Sth} (Fig. S3, *B* and *C*). Besides ∼40% of mutants that contained point mutations in residues involved in HTH-domain sequestration (*e.g.*, E118, E146, D147 or neighboring residues) (Figs. 4*A* and S3*B*), ∼60% of them displayed the substitution F171L in ComR α10 helix (alone or in combination with additional substitutions). These results strongly suggest that residue F171 is pivotal for the activating conformational change of the ComR TPR domain, which corroborates previous observations of F171-Y174 interactions with XIP-1/5 in the activation mechanism (29). In *S. thermophilus*, $ComR_{Sth}$-F171 and Y174 form a hydrophobic cavity at the entry of the XIP-binding pocket where these two residues interact with XIP_{Sth}-L1 as a linear triad of hydrophobic contacts. In *S. vestibularis*, this hydrophobic pocket ($ComR_{Sve}$-Y171 and Y174) is occupied by XIP_{Sve}-M5 with a shift of the side chain of XIP_{Sve}-V1, resulting in a tetra-residue configuration (Fig. 4, *B* and *C*). Although the molecular details by which those residues influence activation are unclear, we previously showed that the double substitution F171A-Y174A in $ComR_{Sth}$ severely reduced activation without a major impact on the binding affinity for XIP_{Sth} (29).

To dissect the respective role of residues F171 and Y174 in $ComR_{Sth}$ activation mechanism, alanine or leucine substitution of each separate residue was generated and compared with the double alanine mutant. Intriguingly, when a relatively high concentration of XIP_{Sth} was added to the medium, none of the single mutants displayed a decrease in light emission as observed for the double mutant (Fig. 5*A*). However, while ComR-Y174A and Y174L maintained a wild-type profile, ComR-F171A and F171L showed an increase in basal activation of ∼5- and ∼160-fold compared with wild-type ComR, respectively (Fig. 5*A*). For ComR-F171L, this high basal activation may explain why the signal is doubled compared with wild-type ComR when XIP_{Sth} was added. These results confirm the screening data by showing the key role played by residue 171 in the conformational change leading to spontaneous activation of ComR.

XIP_{Sth} titration of strains carrying ComR-F171A, ComR-Y174A and the double ComR-F171A-Y174A mutant highlighted that they are differently reduced in their capacity of transcriptional activation compared with wild-type ComR (∼3-, ∼15-, and ∼50-fold higher EC_{50}, respectively) (Fig. 5, *B* and *C*), showing a negative synergic effect of those two mutations on ComR activation. In order to disclose the interplay between these two ComR residues and XIP, the above-mentioned ComR mutants were also tested in the presence of synthetic XIP-A5M. For all the ComR mutants, XIP-A5M enhanced the luminescence signal at a lower concentration than native XIP (Fig. 5, *B* and *C*), indicating that this XIP variant does not strictly require the presence of F171 and/or Y174. However, in contrast to wild-type ComR, none of the mutants could be activated by XIP-A5M at a higher level than the native peptide, which indicates that both F171 and Y174 are required for the optimal activation of the ComR·XIP complex (Fig. 5, *B* and *C*).

These results highlight the contribution of ComR-171–174 and XIP-5 to the activation mechanism and demonstrate that those positions in ComR and XIP can embrace modifications that enhance the activation of the regulatory system.

XIP-A5M activity is modulated by XIP-L1 and ComR-F171

The side chains of residues at positions XIP-1 and 5 display different configurations in *S. thermophilus* and *S. vestibularis*. Both XIP_{Sve}-V1 and XIP_{Sve}-M5 are potentially performing interactions with $ComR_{Sve}$-Y171 and Y174 while only XIP_{Sth}-L1 is interacting with $ComR_{Sth}$-F171 and Y174 (Fig. 4, *B* and *C*).

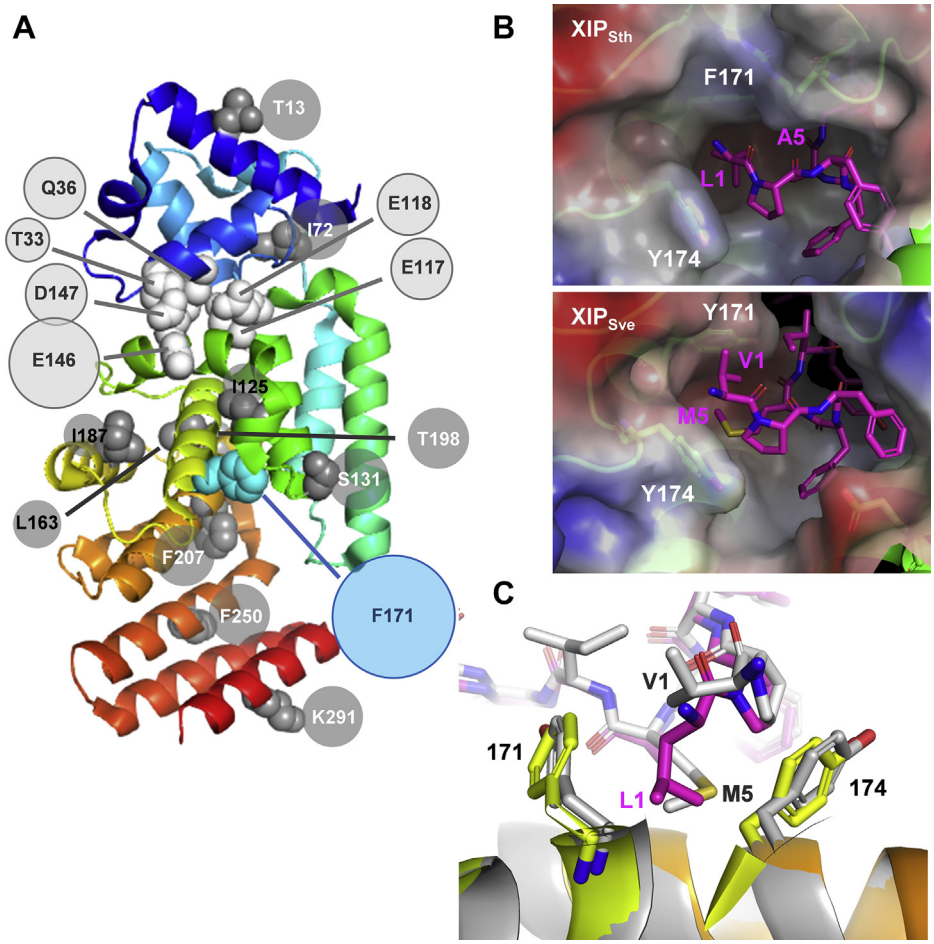

Figure 4. ComR$_{Sth}$ random mutagenesis. *A*, mapping of constitutive mutations on the monomeric apo-ComR. ComR is shown as *cartoon* colored by spectrum from α1 from the HTH domain (*cyan*) to the CAP helix α16 (*red*). Residues substituted in at least two different mutants are labeled. The F171 residue, residues involved in HTH sequestration, and others along the protein are highlighted as *blue*, *white*, and *dark gray spheres*, respectively. The size of the *circle* indicates the occurrence of mutations in each position. *B*, detailed view of the hydrophobic pocket formed by ComR-171 to 174 in *S. thermophilus* (*upper panel*; PDB ID 5JUB (35)) or *S. vestibularis* (*lower panel*; PDB ID 6HUA (37)) occupied by their cognate peptide. The proteins from the ComR·XIP complexes are represented as *cartoon* and *sticks* and colored in *green*, while the peptides are in *purple*. The closed peptide-bound pockets of ComR are shown as surface colored by electrostatic potential (basic regions in *blue*, acidic region in *red*, and nonpolar residues in *white*). Residues XIP-1/5 and ComR-171/174 are labeled. *C*, detailed view of the XIP-1/5 and ComR-171/174 interaction. The 3D structures of complexes ComR$_{Sve}$·XIP$_{Sve}$ (colored as in panel *A*) and ComR$_{Sve}$·XIP$_{Sve}$ (*gray*) are superimposed. ComRs are represented as *cartoon* and XIPs in *sticks*.

First, we evaluated the contribution of XIP$_{Sve}$-V1 and XIP$_{Sve}$-M5 to the activation of ComR$_{Sve}$. For this purpose, XIP$_{Sve}$ variants ΔV1, V1A, and M5A were tested with a *S. thermophilus* reporter strain carrying a substitution of ComR$_{Sth}$ by ComR$_{Sve}$ (30). Activation was completely abolished with XIP$_{Sve}$-ΔV1 (7 aa) and strongly decreased with XIP$_{Sve}$-V1A (∼130-fold) and XIP$_{Sve}$-M5A (∼40-fold) compared with wild-type XIP$_{Sve}$ (Fig. 6*A*). This demonstrates that these two XIP positions are critical to reach the proper activation of the ComR·XIP complex in *S. vestibularis*.

Second, we hypothesized that the XIP$_{Sth}$-A5M may adopt a similar conformation inside the peptide-binding pocket of ComR$_{Sth}$ than observed in ComR$_{Sve}$, thereby reducing the contribution of XIP$_{Sth}$-L1 to the activation of the system. To test this hypothesis, several peptide variants carrying modifications in the N-terminal residue (ΔL1 and L1A) of XIP$_{Sth}$ WT and XIP$_{Sth}$-A5M were compared. All XIP$_{Sth}$-ΔL1 and XIP$_{Sth}$-L1A variants produced a decrease in light emission. The most drastic decrease was observed for XIP$_{Sth}$-ΔL1 (7 aa, ∼90-fold less active), which suggests that the presence of a residue at position 1 is essential for the proper conformation of the peptide and its activity. However, this reduced activation was much less severe when the L1 mutation was combined with A5M (Fig. 6*B*). Using the less active 8-aa variant XIP-L1A (A1–A5) as reference, the addition of substitutions A1L, A5M, and A1L-A5M showed an increased activation of 2.7, 10.4, and 14.4-fold, respectively (Fig. 6*B*). This shows that both leucine L1 and methionine M5 contribute additively to a better ComR$_{Sth}$ activation but with a more predominant role for M5.

Finally, we evaluated the whole range of XIP$_{Sth}$ variants with the ComR-F171A mutant. Notably, when A5M substitution was combined with L1A or ΔL1 mutations, the stimulating effect of A5M was lost in the F171A mutant compared with wild-type ComR$_{Sth}$ (Fig. 6*C*). When using the XIP-L1A as reference, the addition of substitutions A1L, A5M, and A1L-A5M showed an increased activation of 6.8, 1.3, and 14.4-fold, respectively (Fig. 6*C*). While L1 and M5 displayed an additive effect in the activation of wild-type ComR$_{Sth}$, those

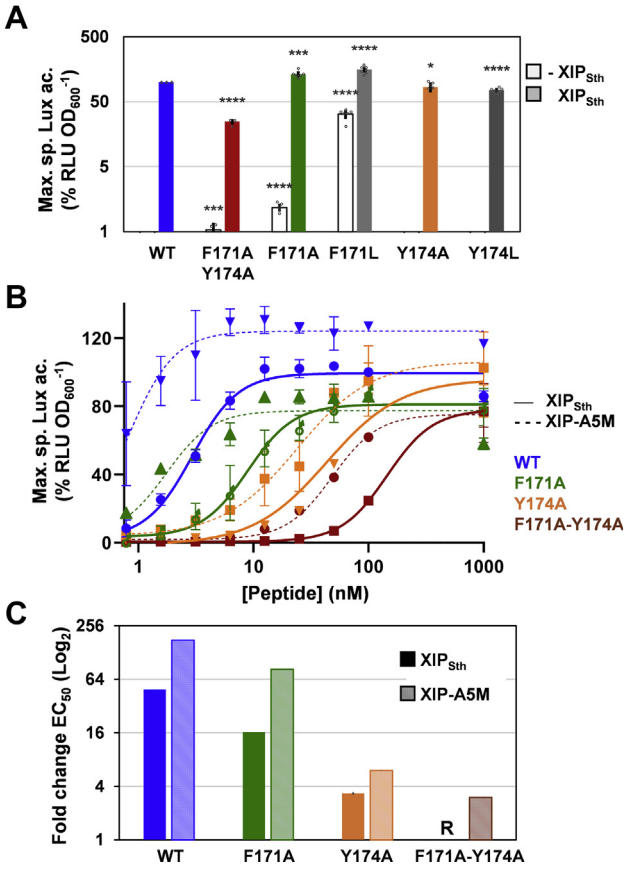

Figure 5. ComR-F171 and Y174 mutants. *A*, maximum specific luciferase activity (% RLU × OD_{600}^{-1}) of *S. thermophilus* Δ*comS* reporter strains producing $ComR_{Sth}$ WT (*blue*), the double mutant ComR-F171A-Y174A (*red*) or the single mutants ComR-F171A (*green*), ComR-F171L (*gray*), ComR-Y174A (*orange*), or ComR-Y174L (*dark gray*) in the absence (−XIP) or presence (+XIP) of XIP_{Sth} WT (100 nM). *B*, dose response of P_{comS} activity upon XIP_{Sth} WT (*solid lines*) or XIP-A5M (*dotted lines*) addition to reporter strains carrying $ComR_{Sth}$ WT (*blue*), ComR-F171A-Y174A (*red*), ComR-F171A (*green*), or ComR-Y174A (*orange*). The monitoring and normalization of luciferase activity were performed as in Figure 2. *C*, fold changes in EC_{50} calculated from the dose response curves shown in panel *B*. The EC_{50} of the double mutant ComR-F171A-Y174A for XIP_{Sth} is used as reference (R) and normalized to 1. Decrease in fold change is representative of an increase in EC_{50}. In *A*, *B*, and *C*, experimental values represent the mean ± SD of at least three independent replicates. In *A*, significant differences ($ComR_{Sth}$ WT as reference in the presence or absence of XIP) calculated by Student unpaired *t* test are indicated (****p-value < 0.0001, ***p-value < 0.001; *p-value < 0.05).

residues are acting synergistically to amplify the activation of the F171A mutant. Moreover, an interaction between XIP_{Sth}-M5 and F171 seems required to observe the boosting effect of M5 when L1 is mutated.

Altogether, these data show that XIP_{Sth}-L1 and XIP_{Sth}-M5 are collaborating in the activation mechanism of $ComR_{Sth}$, most probably by interacting with $ComR_{Sth}$-171 to 174 residues as observed in the crystal structure of $ComR_{Sve}$.

ComR-171/174 – XIP-1/5 interactions remodel a network of aromatic–aromatic interactions

We previously reported that apo-ComR activation by XIP relies on the recruitment of TPR-1 (loop α6–α7) and the CAP helix, the transmission of the shift of helix α7 to an helix-α8 reorientation, which participates to destabilization of helix α9 (break of R39-R51/E117-E118 salt bridges), and finally helix-α9 disruption at position D147 that is needed for HTH-domain release (break of R35/E146-D147 salt bridges) (Fig. 7*A*) (29, 30). However, the results presented here revealed that a key part of the activation mechanism is taking place on the other side of the TPR domain through the interplay between XIP-1/5 and the duo F171-Y174 of helix α10 (Fig. 4).

Using comparative structural analyses and extensive mapping of interactions, we investigated the network of interactions involving residues F/Y171-Y174 in ComR apo-forms and ComR·XIP complexes. The crystal structure of apo-$ComR_{Sth}$ revealed a major (PDB ID 5JUF (33)) and a minor form (Chain A, PDB ID 6QER (34)), in which loop α8 to α9 displayed a completely different conformation (Figs. 7*B* and S4). In the alternative conformation, a large network of predicted aromatic–aromatic interactions that includes residues from loop α8 to α9 ($F132_{Lα8–α9}$ and $W135_{Lα8–α9}$), and other residues from helix α9 ($Y145_{α9}$ and $F149_{α9}$) and helix α10 ($Y168_{α10}$, $F171_{α10}$, $H172_{α10}$ and $Y174_{α10}$) is completely modified, highlighting the high plasticity of loop α8 to α9 residues in Apo-ComR stabilization (Figs. 7*B* and S5). XIP binding through XIP-L1/F171-Y174 interactions induces a new conformational change in loop α8 to α9, which further remodeled this network (Figs. 7*C* and S5; PDB ID 5JUB (35)). The interaction with XIP-L1 (assisted by relay interactions with XIP-P2-F4-Y3) leads to a ∼90° rotation of lateral chains of the $F171_{α10}$-$Y174_{α10}$ duo and a disruption of aromatic–aromatic interaction(s) with $F132_{Lα8–α9}$. This allows the repositioning of $F132_{Lα8–α9}$ at the place of $F171_{α10}$ to form a novel cluster of predicted π-π interactions, including $Y168_{α10}$ and $F171_{α10}$ (Figs. 7*D* and S5). Concomitantly, the interaction $Y168_{α10}$-$I125_{α8}$ is weakened and $W135_{Lα8–α9}$-$H172_{α10}$-$E142_{α9}$/$Y145_{α9}$-$Y168_{α10}$ interactions are disrupted. Those two events participate in helix-α8 shift and destabilization of helix α9, respectively, both required for HTH-domain release (Figs. 7, *C* and *D* and S5). A similar effect could be predicted for the XIP_{Sve}-V1-M5 duo interacting with $ComR_{Sve}$ Y171-Y174 as all the key residues cited above and the predicted network of aromatic–aromatic interactions are largely conserved in ComR of *S. vestibularis* (PDB ID 6HU8 (36) and 6HUA (37)) (Fig. S5). However, in this case and which could be hypothesized for XIP_{Sth}-A5M, the interaction of XIP-1 with F/Y171-Y174 is reinforced by a predicted sulfur–π interaction provided by the methionine at residue XIP-M5 (Fig. S5).

Altogether, these structural comparisons highlight the critical importance of the local remodeling of the network of aromatic–aromatic interactions at the entry of the peptide-binding pocket to allow proper ComR activation.

Discussion

Unveiling the detailed activation mechanism of ComRS systems is an important step toward a better control of DNA transformation as well as understanding their divergent evolution in the context of cell-to-cell communication in

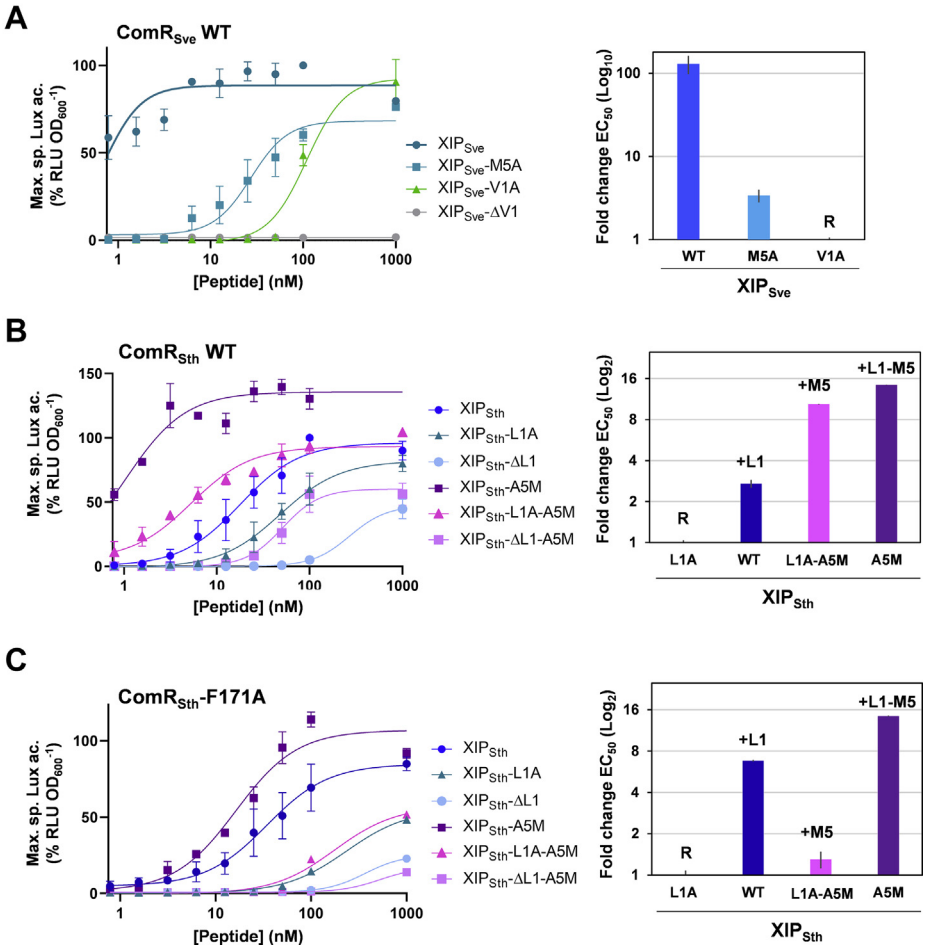

Figure 6. XIP-5 and XIP-1 mutants. *A–C*, dose response of P_{comS} activity (*left panels*) or fold change in EC_{50} (*right panels*) upon addition of synthetic peptide variants carrying XIP-1 and/or XIP-5 substitutions to *S. thermophilus* reporter strains producing $ComR_{Sve}$ WT (*A*), $ComR_{Sth}$ WT (*B*), or ComR-F171A mutant (*C*). The monitoring and normalization of luciferase activity for dose–response curves were performed as in Figure 2. The EC_{50} condition used as reference (fixed to 1) is indicated by R. Experimental values represent the mean ± SD of at least three independent replicates.

streptococci. This work significantly contributes to both aspects, highlighting a critical trigger point involving interactions between the XIP pheromone and its sensor in the activation mechanism.

By analogy, the pheromone–sensor interaction is often simplified and viewed as a selective key–pinhole interaction. However, the situation appears more complex as shown here for the XIP-ComR interaction where XIP is a key with multiple tines whose contacts with its keyhole in ComR will unlock multiple doors of differential importance to allow its dimerization and release of DNA-binding domains. We propose a refined model of the ComRS activation mechanism where the TPR domain is double-locked for its conformational change (Fig. 8, Movies S1 and S2). We previously revealed one of the two unlocking steps involving the toggle switch of TPR-1 (XIP-6 and XIP-8 interactions), CAP recruitment (XIP-3 interaction), and a relay toward a helix-α8 shift contributing to the HTH-domain release (29, 30). Here, we shed light on a second unlocking step that involves the reorganization of TPR-2 (helix-α8 shift and helix-α9 break) through a local remodeling of a network of secondary interactions resulting from contacts with XIP-1/5. While the separate blocking of each remodeling step by targeted mutations of involved residues (*i.e.*, K100A and F171A-Y174A, respectively) was previously shown to strongly decrease XIP-mediated activation (29), the second conformational change is of major importance as a single residue mutation (*i.e.*, F171L) nearly bypassed XIP requirement for activation (Fig. 5*A*). Moreover, the level of constitutive activation is higher than just releasing sequestration of the HTH domain as reported before (29), suggesting a preferential stabilization of the TPR-domain in its active conformation that could for instance promote its dimerization.

Our $ComR_{Sth}$ mutagenesis of aromatic residues F171 and/or Y174 involved in this second unlocking step showed that the progressive decrease of hydrophobic contacts with XIP-1/5 negatively affects XIP activation capacity in a synergistic manner (F171A-Y174A << Y174A < F171A < $ComR_{WT}$) (Fig. 5*C*). Reciprocally, the presence of alanine residues at XIP position 1 and/or 5 in XIP_{Sth} or XIP_{Sve} generated a similar negative effect (Fig. 6*B*), confirming their complementary interdependence in the remodeling of the network of secondary interactions. This predicted network corresponds to a

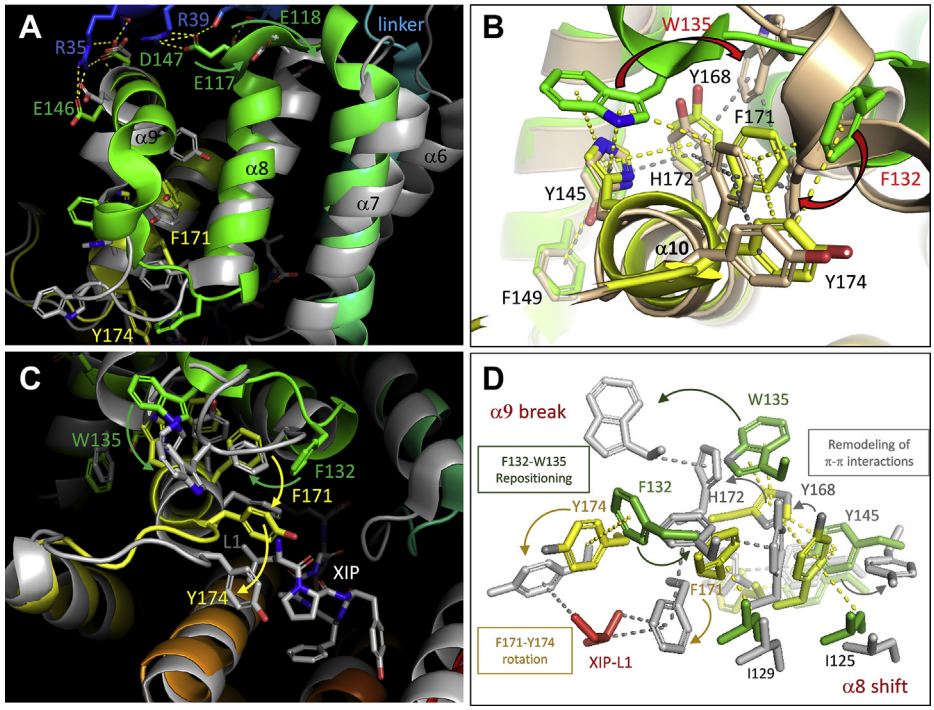

Figure 7. Remodeling of a network of aromatic–aromatic interactions in ComR activation. *A*, XIP-driven reorganization of TPR-1 (α6–α7) and TPR-2 (α8–α9). Apo-$ComR_{Sth}$ (colored by spectrum; PDB ID 5JUF (33)) and $ComR_{Sth}$·XIP_{Sth} complex (*gray*; PDB ID 5JUB (35)) are superimposed. At the *top*, the helix-α8 reorientation is responsible of the break of R39-R51/E117-E118 salt bridges, which contributes to helix–α9 destabilization needed for the HTH domain release (break of R35/E146-D147 salt bridges). At the *bottom*, the remodeling of loop (α8–α9) and the reorientation of aromatic residues F171-Y174 are observed. *B*, F171-Y174 aromatic–aromatic interactions in apo-ComR. The major form (colored by spectrum; PDB ID 5JUF (33)) and a minor form (*beige*; Chain A, PDB ID 6QER (34)) of apo-$ComR_{Sth}$ are superimposed. The network of observed aromatic–aromatic interactions is modified by the repositioning of F132 and W135 from loop α8 to α9 (*red arrows*). Key residues from helix α9 (Y145 and F149) and helix α10 (Y168, F171, H172 and Y174) are indicated. *C*, XIP-driven reorganization of F171-Y174 aromatic–aromatic interactions. Apo-$ComR_{Sth}$ (colored by spectrum; PDB ID 5JUF (33)) and $ComR_{Sth}$·XIP_{Sth} complex (*gray*; PDB ID 5JUB (35)) are superimposed. The rotation of the lateral chains of F171-Y174 in interaction with XIP-L1 and the repositioning of F132 and W135 from loop α8 to α9 are highlighted. *D*, detailed view of XIP-driven reorganization of aromatic lateral chains surrounding F171-Y174. Apo-$ComR_{Sth}$ (colored by spectrum; PDB ID 5JUF (33)) and $ComR_{Sth}$·XIP_{Sth} complex (*gray*; PDB ID 5JUB (35)) are superimposed. The reorientation/repositioning of shown residues participates to helix-α8 shift and helix-α9 break required for HTH domain release. Interactions were mapped using Arpeggio (http://biosig.unimelb.edu.au/arpeggioweb/) (52).

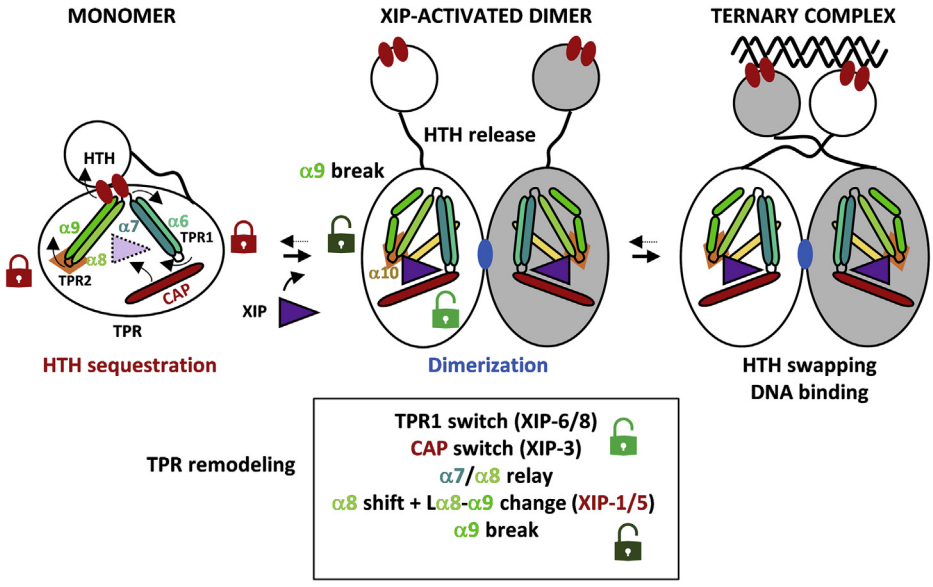

Figure 8. Refined model of ComR activation mechanism. The HTH and TPR domains of the protein are shown with the flexible linker. TPR-1 (α6–α7), TPR-2 (α8–α9), α10, and CAP helix, directly implicated in XIP binding and release of the ComR locked state, are shown as *sticks* and labeled. Helices are colored as in Figure 4. *Red* and *blue ellipses* represent residues involved in HTH sequestration and TPR dimerization, respectively. The *orange diamond* represents local aromatic–aromatic interactions that are remodeled through XIP-1/5-F/Y171-Y178 interactions.

very large cluster of π-π (12–14) and C-H···π (9–11) interactions, buried in the hydrophobic core of ComR and interconnecting helices α8, α9, and α10 (Fig. S5). This network is remodeled upon XIP interaction, which allows the rearrangement of loop α8 to α9 and TPR conformational change (Fig. S5). A range of mutagenesis works have shown that these aromatic clusters are very sensitive to destabilization by simple conservative mutation (*e.g.*, aromatic residue to leucine) or subtle reorientation of aromatic rings (38–41). Similarly, our random mutagenesis revealed that the ComR-F171$_{\alpha10}$ residue is pivotal for maintaining the nonactive status of the apo form. Its substitution by a conservative leucine residue has a dramatic effect on the differential stability between the TPR-domain conformations, leading to a constitutively active ComR. Moreover, since the F171A mutant displayed a lower constitutive activation, this active conformation is probably preferentially stabilized by hydrophobic contacts(s) involving L171. A possible scenario is the positioning of L171 in a similar configuration than F171 in the activated form with its stabilization through interactions with F132$_{L\alpha8-\alpha9}$ and Y168$_{\alpha10}$, which is probably less efficient with an alanine residue (Fig. S5). In this case, the L171 mutation may somehow mimic the XIP-L1/ComR-F171 interaction, resulting in a similar reorganization of the aromatic–aromatic interaction network as reported for the active conformation (Fig. S5). Our mutagenesis work also showed that Y174 seems to play a less important role in the differential stabilization between apo and holo states, probably due to the external position of this residue in the network (Figs. 5, *A* and *B* and S5). It is interesting to note that mutating residue I125$_{\alpha8}$ into leucine, which interacts with Y168$_{\alpha10}$ and thus participates in the network by anchoring of α8 to α10 (Fig. 7*D*), also leads to a constitutive activation but at a lower level than F171L (Figs. S3 and S5). In contrast to the negative effect on protein functionality generally assigned to disruption of aromatic clusters (38, 39, 41), our results show that the fine-tuning of hydrophobic contacts between XIP and ComR-F171-Y174 in the peptide-binding pocket positively remodel ComR for its activation.

The XIP semirational mutagenesis used during this work also revealed that the efficiency of ComRS activation can be significantly improved by a modified pheromone with a reactivity in the sub-nanomolar range and a dramatic increase in DNA transformation efficiency (Fig. 2, *A* and *D*). To our knowledge, such improvement of the activation of a member of the (R)RNPP family has never been reported so far. The higher activation of ComR$_{Sth}$ by the presence of a single substitution of an alanine by a methionine at XIP-5 results probably from mimetic interactions, which are taking place at the entry of the XIP-binding pocket in *S. vestibularis* ComR (Fig. 4, *A* and *B*). Since methionine is more hydrophobic than alanine, XIP-A5M is less stable in water and its desolvation upon binding to ComR may account for its increased affinity. Indeed, a difference in desolvation energy between 1.2 and 1.4 kcal/mol is expected upon alanine to methionine substitution (42), resulting in a maximal seven- to ten-fold increase in affinity. The flexibility of the linear methionine side chain should help accommodating the residue in the binding pocket and minimizing steric hindrance in the complex. Besides flexibility and hydrophobicity, methionine is also quite unique in its ability to perform sulfur–π interaction(s) that may bring additional stabilization of ∼1.0 to 1.5 kcal/mol (43). Such interaction is predicted between XIP$_{Sve}$-M5 and ComR$_{Sve}$-Y174 (Fig. S5) and may take place similarly in ComR$_{Sth}$ although it may require structural rearrangement. Sulfur–π interactions have been reported to strongly contribute to protein stabilization, receptor–ligand or protein–protein interactions, and more recently to ion channel gating (43–45). Finally, the triad aromatic-Met-aromatic (named Aro-Met-Aro) has recently been identified as a novel motif in numerous crystal structures (46). Here, an intermolecular Aro-Met-Aro bridging interaction may further stabilize the XIP-M5 and ComR-Y/F171-Y174 complex.

ComRS systems have divergently evolved in streptococci with the apparition of pherotypes that can largely differ, even between members of the same *streptococcus* group (19). In salivarius streptococci, two well-separated pherotypes are found between *S. thermophilus*/*S. salivarius* (named type Ia) and *S. vestibularis* (type Ib) (prototypes in Fig. 1*B*) (19, 30). Although no XIP type Ia with a methionine at position 5 has been found until now, some XIPs exhibit a threonine at that position in type Ia or an isoleucine in type Ib (30). Interestingly, the natural variation A5T is neutral compared with the most represented A5 residue in XIP type Ia (Fig. 2*C*). However, in a similar situation to XIP$_{Sth}$-A5M, the A5I substitution improved transcriptional activation but at a lower level than A5M (Fig. 2*C*). These observations corroborate the relative importance of XIP-1/5 in the activation of ComR$_{Sve}$ *versus* ComR$_{Sth}$ (Fig. 6, *A* and *B*) and suggest that pheromones or ComR-pheromone couples found in nature are not necessarily the most active ones. In the same vein, we observed a growth defect when the more active peptide is added to the medium or is natively produced (Fig. 2*B*). It is important to recall that competence development is a tightly controlled process that is generally activated during a short time window (13). It is also well documented that the process is not only energetically expensive but can also disturb cell division and chromosome integrity when dysregulated (9, 13). These physiological disturbances probably explain evolutionary constrains on the ComRS system. They prevent hyperactive systems in order to minimize the decrease in fitness when competence is over-triggered and ensure its tight control.

To conclude, our results shed light on a novel trigger point in the ComR activation mechanism and its evolutionary consequences for the fine-tuning of competence control. Besides, this work also offers biotechnological opportunities to better stimulate natural transformation for engineering food-associated streptococci or improving peptide-based expression systems. As ComR stimulates the production of antimicrobials (bacteriocins) in many streptococci (31, 32), optimized pheromone might alternatively be exploited to bolster interspecies predation and kill pathogenic bacteria at the infection site.

Experimental procedures

Bacterial strains, plasmids, and oligonucleotides

Bacterial strains, plasmids, and oligonucleotides used in this study are listed in Tables S1 and S2. The primers used in this study were purchased from Eurogentec.

Growth conditions

S. thermophilus LMD-9 and derivatives were grown at 37 °C without shaking in M17 broth (Difco Laboratories Inc) or in CDM (47) supplemented with 1% glucose [w/v] (M17 and CDMG broth, respectively). *Escherichia coli* was grown in LB medium with shaking at 37 °C. When required, chloramphenicol (3.5 or 5 μg ml^{-1} for *S. thermophilus*), erythromycin (2.5 μg ml^{-1} for *S. thermophilus*), or ampicillin (200 μg ml^{-1} for *E. coli*) was added to the media. Plates inoculated with *S. thermophilus* cells were incubated anaerobically (BBL GasPak systems, Becton Dickinson) at 37 °C.

Preparation of XIP peptides

Synthetic XIP octapeptides, polyG-XIP octapeptides, and FITC N-labeled nonapeptides were supplied by Peptide 2.0 or GeneScript (Table S3). They were resuspended in bi-distillated water, except FITC N-labeled nonapeptides that were solubilized in 100% dimethyl sulfoxide (DMSO) (vol/vol). Final concentration was quantified using a Nanodrop apparatus (Thermo Fisher Scientific).

Natural DNA transformation

To induce competence, overnight *S. thermophilus* precultures grown in CDMG were diluted in semiskimmed milk at a final OD_{600} of 0.05. After an incubation of 75 min at 37 °C, 1 μM of XIP_{Sth} WT and linear DNA fragments were added. Cells were grown for 4 h at 37 °C before plating on selective M17G agar and incubation in anaerobic conditions. Positive candidates were confirmed by streaking on selective plates and verified by PCR and sequencing (18, 48).

Transformation efficiency assays were performed as reported above by adding 1 μg of multimeric and circular plasmid pGhost9-core, together with XIP_{Sth} (100 nM) when needed. All incubation steps were performed at 30 °C to allow plasmid replication. The plasmid was purified from *E. coli* using a Maxiprep Kit for low-copy plasmids (Thermo Fisher Scientific) following manufacturer' instructions. Transformation efficiency corresponds to the total number of transformants (erythromycin-resistant colony-forming units) per ml.

Construction of comS and comR mutant strains

S. thermophilus strain LL30 (LMD-9 derivative) expressing *comS-11aa* was constructed as follows. Four PCR fragments with the following features were joined to replace *comS* by *comS-11aa*: fragment 1 with *comR* and P_{comS} (primers #1 and #2), fragment 2 with the $comS_{\Delta 2-13}$ (primers #3 and #4), fragment 3 with the P_{32}-*cat* cassette (primers #6 and #7), and fragment 4 with the ∼1-kb *comS* downstream region (primers #5 and #25). With the exception of the P_{32}-*cat* cassette amplified from strain LF134 (19), strain LMD-9 was used as template to amplify the other fragments.

Strain LL31 containing a replacement of *comS* by a P_{comS}-*cat* fusion was constructed by joining two PCR fragments: fragment 1 with *comR*-P_{comS} (primers #1 and #12; LMD-9 as template) and fragment 2 with the promoter-less *cat* gene (primers #11 and #25; LF134 as template).

Strains LL32 and LL33 expressing *comS-24aa-A5M* and *comS-24aa-L1V-A5M*, respectively, were constructed by joining two PCR fragments: fragment 1 with *comR*-P_{comS} and *comS′* encoding N-terminal ComS-16aa (primers #1 and #8; LMD-9 as template) and fragment 2 with point mutation(s) A5M without or with L1V (primers #9 or #10, and #25, respectively; LL30 as template).

Strains LL40, LL42, LL42, and LL43 expressing *comR-F171A*, *comR-F171L*, *comR-Y174A*, and *comR-Y174L*, respectively, were constructed by joining two PCR fragments: fragment 1 with a ∼1-kb *comR* upstream region and the 5′end of *comR* (primers #24 and #17, #19, #21, or #23, respectively; LMD-9 as template), and fragment 2 with the 3′ end of *comR*, *comS* substituted by P_{32}-*cat*, and ∼1-kb downstream region of *comS* (primers #31 and #16, #18, #20, or #22, respectively; LF134 as template). Internal primers enclosed the point mutation in each case.

The different fragments were joined by overlapping PCR using external primers and the full-length product was transformed by natural transformation in the reporter strain LF121 (P_{comS}-*luxAB*) for chromosomal replacement by double homologous recombination (19). For strain LL31, transformants were selected on plates containing both chloramphenicol and XIP_{Sth} 1 μM. Then, this strain was validated as chloramphenicol sensitive in absence of XIP_{Sth}.

Semirational XIP mutagenesis in S. thermophilus

In order to perform the peptide screening, strain LL34 containing both P_{comS}-*cat* and P_{comS}-*comS-11aa* was constructed. Three PCR fragments with the following features were joined: fragment 1 with *comR* and P_{comS}-*cat* (primers #1 and #7; LL31 as template), fragment 2 with P_{comS}-*comS-11aa* (primers #14 and #15; LL30 as template), and fragment 3 with ∼1-kb *comS* downstream region (primers #13 and #25, LMD-9 as template). Overlapping PCR and natural transformation in LF121 were performed as reported above.

To generate the DNA library encoding semirandomized peptide variants, two PCR fragments were jointed: fragment 1 with *comR*-P_{comS}-*cat* (primers #1 and #33; LL34 as template) and fragment 2 with the semi-randomized DNA stretch and ∼1 kb *comS*-downstream region (primers #32 and #25; LL34 as template). Primer #32 included a semidegenerated sequence allowing any amino acid exchange between XIP_{Sth} and XIP_{Sve} sequences (8 aa). After overlapping PCR to join the fragments, the final PCR product was transformed in the reporter strain LF121. Chloramphenicol-resistant candidates were restreaked on selective medium and analyzed by sequencing and luciferase activation.

Random ComR *mutagenesis in* S. thermophilus

To generate the *comR* library, random $ComR_{Sth}$ mutagenesis was achieved by error-prone PCR allowing 0 to 3 mutations per kb (49). The ComR mutant library was produced by amplifying the $comR_{Sth}$ gene with primers #28 and #29 (LMD-9 as template). The library was included in a final overlapping PCR product obtained from three PCR fragments: fragment 1 with a ~1-kb *comR* upstream region (primers #24 and #30, LMD-9 as template), fragment 2 with the $comR_{Sth}$ random library, and fragment 3 with a ~1-kb downstream region of P_{comS}-*cat* cassette (primers #31 and #25; LL31 as template). The final PCR product carrying *comR* mutants was transformed in the reporter strain LF121 (19). Natural transformation was performed as reported above and transformants were selected on chloramphenicol (3.5 μg ml^{-1}), restreaked on selective medium with and without XIP_{Sth} 1 μM, and tested for luciferase activity.

Measurements of luciferase activity

Luciferase assays were performed as previously described (19). Overnight precultures were diluted to a final OD_{600} of 0.05 and culture samples incubated in a sterile covered white microplate with a transparent bottom (Greiner). Growth and luciferase activity (expressed in relative light units [RLUs]) of the cultures were monitored after addition or in absence of synthetic XIP peptide at 10 min intervals during at least 8 h in a multiwell plate reader (Hidex Sense, Hidex). When peptides were titrated, 0, 0.78, 1.56, 3.12, 6.25, 12.5, 25, 50, 100, and 1000 nM were added to the medium. In order to calculate EC_{50} values (peptide concentration for a half maximum response), maximum luciferase activity values were fitted to Hill equation:

$$L = \frac{L_{max} \times [XIP]^n}{(EC_{50})^n + [XIP]^n}$$

where L is the luciferase activity, [XIP] is the XIP concentration, and *n* is the Hill coefficient. Curves were fitted with the GraphPad Prism software v.9.0.1 (GraphPad Software, Inc).

ComR purification

E. coli strain TOP10 (Invitrogen) electrotransformation of plasmid pBADcomRSth-strep, purification of $ComR_{Sth}$-StreptagII protein, and protein storage were performed as described previously (30). Protein purity was analyzed by SDS-PAGE and protein concentration was measured using a Nanodrop apparatus (Thermo Fisher Scientific).

Fluorescence polarization assays

FP assays were performed as previously described (30, 32). Threefold serial dilutions of purified ComR (initial concentration of 1 μM) were mixed with a FITC N-labeled version (9 aa) of XIP peptides (ILPYFAGCL and ILPYFMGCL) at a fixed concentration of 30 nM. The samples were incubated for 10 min at 30 °C in black 96-well plates (Greiner). Anisotropic measurements were performed in a multiwell plate reader (Hidex Sense, Hidex) in polarization mode with 485/10-nm and 535/20-nm excitation and emission filters, respectively. EC_{50} values of curves that reached saturation were obtained by fitting the plots to the Hill equation:

$$F = \frac{F_{max} \times [XIP]^n}{(EC_{50})^n + [XIP]^n}$$

where F is the polarized fluorescence, [XIP] is the XIP concentration, and *n* is the Hill coefficient. Curves were fitted with the GraphPad Prism software v.9.0.1 (GraphPad Software, Inc).

In the case of competition assays, a fixed concentration of ComR (250 nM) and FITC N-labeled XIP peptide (30 nM) were incubated with twofold serial dilutions of unlabeled XIP variant (initial concentration of 5 μM). Plots were fitted by using GraphPad Prisma software to calculate IC_{50} values (half-maximal inhibitory peptide concentration).

Single-molecule force spectroscopy

Gold-coated glass coverslips and cantilevers (OMCL-TR4, Olympus Ltd; nominal spring constant ~0.02 N m^{-1}) were immersed overnight in an ethanol solution containing 1 mM of 10% 16- mercaptododecahexanoic acid/90% 1-mercapto-1-undecanol (Sigma), rinsed with ethanol and dried with N_2. Substrates and cantilevers were then immersed for 30 min into a solution containing 10 mg ml^{-1} *N*-hydroxysuccinimide (NHS) and 25 mg ml^{-1} 1-ethyl-3-(3-dimethylaminopropyl)-carbodiimide (EDC) (Sigma), rinsed with Ultrapure water (ELGA LabWater), incubated with 0.1 mg ml^{-1} ComR or polyG-XIP_{Sth}, polyG-XIP-A5M, or polyG-XIP_{Sve} peptides for 1 h, rinsed further with PBS buffer, and then immediately used without dewetting.

For experiments of single-molecule force spectroscopy, ComR-functionalized surfaces and functionalized cantilevers with polyG-peptides were prepared as described above. Measurements were performed at room temperature in PBS with a Force Robot 300 AFM (JPK Instruments). Multiple (32 × 32) force–distance curves were recorded on areas of 500 by 500 nm^2 with an applied force of 250 pN, a constant approach, and retraction speed of 1000 nm s^{-1}. Histograms were generated by considering, for every curve, the force and the distance of the last rupture event. The spring constants of the cantilevers were measured by the thermal noise method (50). Data were analyzed with the data processing software from JPK Instruments.

Electrophoretic mobility shift assays

EMSA assays were performed as previously described (19, 30). A fixed concentration of purified ComR protein (1 μM) was mixed with twofold serial dilutions of the XIP variant (initial concentration of 2 μM) together with a 40-bp dsDNA fragment (20 ng) carrying the ComR box of PcomS coupled to the Cy3 fluorophore. Negative controls were performed in absence of XIP. Mix was incubated at 37 °C for 10 min prior to analysis on a native 4 to 20% gradient gel (iD PAGE gel;

Eurogentec) and DNA complexes were detected by fluorescence on the Ettan DIGE Imager with bandpass excitation and emission filters of 540/25 and 595/25 nm, respectively (GE Healthcare). Double-stranded DNA fragment was obtained from annealing of single-stranded Cy3-labeled (at 5′ end) and unlabeled oligonucleotides.

Multiple sequence alignments, phylogenetic analysis, and structure visualization

Multiple alignment of screened XIP variants was generated with Clustal Omega (https://www.ebi.ac.uk/Tools/msa/clustalo/) (51). The formatting of the alignment was performed with CLC Main Workbench 7 (https://www.qiagenbioinformatics.com/). The figures with structural elements were prepared by using the graphic software PyMol (http://www.pymol.org/).

Data availability

All data are contained within the article and the supporting information.

Supporting information—This article contains supporting information (18, 19, 29, 30, 33–37, 52).

Acknowledgments—This work was supported by the Belgian National Fund for Scientific Research (FNRS, grant PDR T.0110.18), the Interuniversity Attraction Poles (IAP, grant P17/28) Program of the Belgian Science Policy Office (BELSPO), and the Concerted Research Actions (ARC, grant 17/22-084) from Federation Wallonia-Brussels.

Author contributions—L. L.-G., J. M., Y. F. D., P. S., and P. H. conceptualization; L. L.-G., I. E., D. D., F. V., and P. H. formal analysis; P. H. funding acquisition; L. L.-G., I. E., D. D., and F. V. investigation; L. L.-G., I. E., and F. V. methodology; P. H. project administration; L. L.-G., P. S., and P. H. supervision; P. S., S. N., and P. H. validation; L. L.-G., F. V., P. S., S. N., and P. H. visualization; L. L.-G. and F. V. writing—original draft; J. M., Y. F. D., P. S., S. N., and P. H. writing—review and editing.

Conflict of interest—P. H. and Y. F. D. are research directors at FNRS. All other authors declare that they have no conflicts of interest with the contents of this article.

Abbreviations—The abbreviations used are: AFM, atomic force microscopy; CAP helix, capping helix α16; $ComR_{Sth}$, *Streptococcus thermophilus* ComR; $ComR_{Sve}$, *Streptococcus vestibularis* ComR; CSP, competence-stimulating peptide; FP, fluorescence polarization; HTH, helix-turn-helix; P_{comS}, *comS* promoter; RLU, relative light unit; (R)RNPP, (Rgg,) Rap, NprR, PlcR, and PrgX; TPR, tetratricopeptide repeat; XIP, SigX-inducing peptide; XIP_{Sth}, *Streptococcus thermophilus* XIP; XIP_{Sve}, *Streptococcus vestibularis* XIP.

References

1. Gogarten, J. P., Doolittle, W. F., and Lawrence, J. G. (2002) Prokaryotic evolution in light of gene transfer. *Mol. Biol. Evol.* **19**, 2226–2238
2. Claverys, J. P., Prudhomme, M., Mortier-Barriere, I., and Martin, B. (2000) Adaptation to the environment: *Streptococcus pneumoniae*, a paradigm for recombination-mediated genetic plasticity? *Mol. Microbiol.* **35**, 251–259
3. Johnston, C., Martin, B., Fichant, G., Polard, P., and Claverys, J. P. (2014) Bacterial transformation: Distribution, shared mechanisms and divergent control. *Nat. Rev. Microbiol.* **12**, 181–196
4. Lorenz, M. G., and Wackernagel, W. (1994) Bacterial gene transfer by natural genetic transformation in the environment. *Microbiol. Rev.* **58**, 563–602
5. Lattar, S. M., Wu, X., Brophy, J., Sakai, F., Klugman, K. P., and Vidal, J. E. (2018) A mechanism of unidirectional transformation, leading to antibiotic resistance, occurs within nasopharyngeal pneumococcal biofilm consortia. *mBio* **9**, e00561-18
6. Blokesch, M. (2016) Natural competence for transformation. *Curr. Biol.* **26**, R1126–R1130
7. Claverys, J. P., Martin, B., and Polard, P. (2009) The genetic transformation machinery: Composition, localization, and mechanism. *FEMS Microbiol. Rev.* **33**, 643–656
8. Moradigaravand, D., and Engelstadter, J. (2013) The evolution of natural competence: Disentangling costs and benefits of sex in bacteria. *Am. Nat.* **182**, E112–E126
9. Zaccaria, E., Wells, J. M., and van Baarlen, P. (2016) Metabolic context of the competence-induced checkpoint for cell replication in *Streptococcus suis*. *PLoS One* **11**, e0153571
10. Haijema, B. J., Hahn, J., Haynes, J., and Dubnau, D. (2001) A ComGA-dependent checkpoint limits growth during the escape from competence. *Mol. Microbiol.* **40**, 52–64
11. Mirouze, N., Berge, M. A., Soulet, A. L., Mortier-Barriere, I., Quentin, Y., Fichant, G., Granadel, C., Noirot-Gros, M. F., Noirot, P., Polard, P., Martin, B., and Claverys, J. P. (2013) Direct involvement of DprA, the transformation-dedicated RecA loader, in the shut-off of pneumococcal competence. *Proc. Natl. Acad. Sci. U. S. A.* **110**, E1035–E1044
12. Weng, L., Piotrowski, A., and Morrison, D. A. (2013) Exit from competence for genetic transformation in *Streptococcus pneumoniae* is regulated at multiple levels. *PLoS One* **8**, e64197
13. Fontaine, L., Wahl, A., Flechard, M., Mignolet, J., and Hols, P. (2015) Regulation of competence for natural transformation in streptococci. *Infect. Genet. Evol.* **33**, 343–360
14. Lee, M. S., and Morrison, D. A. (1999) Identification of a new regulator in *Streptococcus pneumoniae* linking quorum sensing to competence for genetic transformation. *J. Bacteriol.* **181**, 5004–5016
15. Havarstein, L. S., Coomaraswamy, G., and Morrison, D. A. (1995) An unmodified heptadecapeptide pheromone induces competence for genetic transformation in *Streptococcus pneumoniae*. *Proc. Natl. Acad. Sci. U. S. A.* **92**, 11140–11144
16. Martin, B., Soulet, A. L., Mirouze, N., Prudhomme, M., Mortier-Barriere, I., Granadel, C., Noirot-Gros, M. F., Noirot, P., Polard, P., and Claverys, J. P. (2013) ComE/ComE∼P interplay dictates activation or extinction status of pneumococcal X-state (competence). *Mol. Microbiol.* **87**, 394–411
17. Pestova, E. V., Havarstein, L. S., and Morrison, D. A. (1996) Regulation of competence for genetic transformation in *Streptococcus pneumoniae* by an auto-induced peptide pheromone and a two-component regulatory system. *Mol. Microbiol.* **21**, 853–862
18. Fontaine, L., Boutry, C., de Frahan, M. H., Delplace, B., Fremaux, C., Horvath, P., Boyaval, P., and Hols, P. (2010) A novel pheromone quorum-sensing system controls the development of natural competence in *Streptococcus thermophilus* and *Streptococcus salivarius*. *J. Bacteriol.* **192**, 1444–1454
19. Fontaine, L., Goffin, P., Dubout, H., Delplace, B., Baulard, A., Lecat-Guillet, N., Chambellon, E., Gardan, R., and Hols, P. (2013) Mechanism of competence activation by the ComRS signalling system in streptococci. *Mol. Microbiol.* **87**, 1113–1132
20. Gardan, R., Besset, C., Gitton, C., Guillot, A., Fontaine, L., Hols, P., and Monnet, V. (2013) Extracellular life cycle of ComS, the competence-stimulating peptide of *Streptococcus thermophilus*. *J. Bacteriol.* **195**, 1845–1855
21. Khan, R., Rukke, H. V., Ricomini Filho, A. P., Fimland, G., Arntzen, M. O., Thiede, B., and Petersen, F. C. (2012) Extracellular identification of a

processed type II ComR/ComS pheromone of *Streptococcus mutans*. *J. Bacteriol.* **194**, 3781–3788
22. Mashburn-Warren, L., Morrison, D. A., and Federle, M. J. (2010) A novel double-tryptophan peptide pheromone controls competence in *Streptococcus* spp. via an Rgg regulator. *Mol. Microbiol.* **78**, 589–606
23. Declerck, N., Bouillaut, L., Chaix, D., Rugani, N., Slamti, L., Hoh, F., Lereclus, D., and Arold, S. T. (2007) Structure of PlcR: Insights into virulence regulation and evolution of quorum sensing in Gram-positive bacteria. *Proc. Natl. Acad. Sci. U. S. A.* **104**, 18490–18495
24. Do, H., and Kumaraswami, M. (2016) Structural mechanisms of peptide recognition and allosteric modulation of gene regulation by the RRNPP family of quorum-sensing regulators. *J. Mol. Biol.* **428**, 2793–2804
25. Grenha, R., Slamti, L., Nicaise, M., Refes, Y., Lereclus, D., and Nessler, S. (2013) Structural basis for the activation mechanism of the PlcR virulence regulator by the quorum-sensing signal peptide PapR. *Proc. Natl. Acad. Sci. U. S. A.* **110**, 1047–1052
26. Neiditch, M. B., Capodagli, G. C., Prehna, G., and Federle, M. J. (2017) Genetic and structural analyses of RRNPP intercellular peptide signaling of Gram-positive bacteria. *Annu. Rev. Genet.* **51**, 311–333
27. Shanker, E., Morrison, D. A., Talagas, A., Nessler, S., Federle, M. J., and Prehna, G. (2016) Pheromone recognition and selectivity by ComR proteins among *Streptococcus* species. *PLoS Pathog.* **12**, e1005979
28. Zouhir, S., Perchat, S., Nicaise, M., Perez, J., Guimaraes, B., Lereclus, D., and Nessler, S. (2013) Peptide-binding dependent conformational changes regulate the transcriptional activity of the quorum-sensor NprR. *Nucleic Acids Res.* **41**, 7920–7933
29. Talagas, A., Fontaine, L., Ledesma-Garcia, L., Mignolet, J., Li de la Sierra-Gallay, Lazar, N., Aumont-Nicaise, M., Federle, M. J., Prehna, G., Hols, P., and Nessler, S. (2016) Structural insights into streptococcal competence regulation by the cell-to-cell communication system ComRS. *PLoS Pathog.* **12**, e1005980
30. Ledesma-Garcia, L., Thuillier, J., Guzman-Espinola, A., Ensinck, I., Li de la Sierra-Gallay, Lazar, N., Aumont-Nicaise, M., Mignolet, J., Soumillion, P., Nessler, S., and Hols, P. (2020) Molecular dissection of pheromone selectivity in the competence signaling system ComRS of streptococci. *Proc. Natl. Acad. Sci. U. S. A.* **117**, 7745–7754
31. Mignolet, J., Fontaine, L., Sass, A., Nannan, C., Mahillon, J., Coenye, T., and Hols, P. (2018) Circuitry rewiring directly couples competence to predation in the gut dweller *Streptococcus salivarius*. *Cell Rep.* **22**, 1627–1638
32. Mignolet, J., Cerckel, G., Damoczi, J., Ledesma-Garcia, L., Sass, A., Coenye, T., Nessler, S., and Hols, P. (2019) Subtle selectivity in a pheromone sensor triumvirate desynchronizes competence and predation in a human gut commensal. *Elife* **8**, e47139
33. [dataset] Talagas, A., Fontaine, L., Ledesma-Garcia, L., Li de la Sierra-Gallay, I., Hols, P., and Nessler, S. (2016) Crystal structure of the apo form of ComR from S. thermophilus. *Protein Data Bank*, 5JUF
34. [dataset] Thuillier, J., and Nessler, S. (2019) Apo form of ComR from S. thermophilus in space group C2. *Protein Data Bank*, 6QER
35. [dataset] Talagas, A., Fontaine, L., Ledesma-Garcia, L., Li de la Sierra-Gallay, I., Hols, P., and Nessler, S. (2016) Crystal structure of ComR from S. thermophilus in complex with DNA and its signalling peptide ComS. *Protein Data Bank*, 5JU
36. [dataset] Nessler, S., Thuillier, J., Ledesma-Garcia, L., and Hols, P. (2018) Apo form of the competence regulator ComR from Streptococcus vestibularis. *Protein Data Bank*, 6HU8
37. [dataset] Nessler, S., Thuillier, J., Ledesma-Garcia, L., and Hols, P. (2018) The competence regulator ComR from Streptococcus vestibularis in complex with its cognate signaling peptide XIP. *Protein Data Bank*, 6HUA
38. Chatterjee, K. S., Tripathi, V., and Das, R. (2019) A conserved and buried edge-to-face aromatic interaction in small ubiquitin-like modifier (SUMO) has a role in SUMO stability and function. *J. Biol. Chem.* **294**, 6772–6784
39. Frank, B. S., Vardar, D., Buckley, D. A., and McKnight, C. J. (2002) The role of aromatic residues in the hydrophobic core of the villin headpiece subdomain. *Protein Sci.* **11**, 680–687
40. Hillier, B. J., Rodriguez, H. M., and Gregoret, L. M. (1998) Coupling protein stability and protein function in Escherichia coli CspA. *Fold. Des.* **3**, 87–93
41. Serrano, L., Bycroft, M., and Fersht, A. R. (1991) Aromatic-aromatic interactions and protein stability. Investigation by double-mutant cycles. *J. Mol. Biol.* **218**, 465–475
42. Wimley, W. C., Creamer, T. P., and White, S. H. (1996) Solvation energies of amino acid side chains and backbone in a family of host-guest pentapeptides. *Biochemistry* **35**, 5109–5124
43. Valley, C. C., Cembran, A., Perlmutter, J. D., Lewis, A. K., Labello, N. P., Gao, J., and Sachs, J. N. (2012) The methionine-aromatic motif plays a unique role in stabilizing protein structure. *J. Biol. Chem.* **287**, 34979–34991
44. Spencer, D. S., and Stites, W. E. (1996) The M32L substitution of staphylococcal nuclease: Disagreement between theoretical prediction and experimental protein stability. *J. Mol. Biol.* **257**, 497–499
45. Yeung, P. S., Ing, C. E., Yamashita, M., Pomes, R., and Prakriya, M. (2020) A sulfur-aromatic gate latch is essential for opening of the Orai1 channel pore. *Elife* **9**, e60751
46. Weber, D. S., and Warren, J. J. (2019) The interaction between methionine and two aromatic amino acids is an abundant and multifunctional motif in proteins. *Arch. Biochem. Biophys.* **672**, 108053
47. Letort, C., and Juillard, V. (2001) Development of a minimal chemically-defined medium for the exponential growth of *Streptococcus thermophilus*. *J. Appl. Microbiol.* **91**, 1023–1029
48. Fontaine, L., Dandoy, D., Boutry, C., Delplace, B., de Frahan, M. H., Fremaux, C., Horvath, P., Boyaval, P., and Hols, P. (2010) Development of a versatile procedure based on natural transformation for marker-free targeted genetic modification in *Streptococcus thermophilus*. *Appl. Environ. Microbiol.* **76**, 7870–7877
49. Cirino, P. C., Mayer, K. M., and Umeno, D. (2003) Generating mutant libraries using error-prone PCR. *Methods Mol. Biol.* **231**, 3–9
50. Hutter, J., and Bechhoefer, J. (1993) Calibration of atomic-force microscope tips. *Rev. Sci. Instrum.* **64**, 1863–1873
51. Sievers, F., Wilm, A., Dineen, D., Gibson, T. J., Karplus, K., Li, W., Lopez, R., McWilliam, H., Remmert, M., Soding, J., Thompson, J. D., and Higgins, D. G. (2011) Fast, scalable generation of high-quality protein multiple sequence alignments using Clustal Omega. *Mol. Syst. Biol.* **7**, 539
52. Jubb, H. C., Higueruelo, A. P., Ochoa-Montano, B., Pitt, W. R., Ascher, D. B., and Blundell, T. L. (2017) Arpeggio: A web server for calculating and visualising interatomic interactions in protein structures. *J. Mol. Biol.* **429**, 365–371
53. Sayle, R. A., and Milner-White, E. J. (1995) RASMOL: Biomolecular graphics for all. *Trends Biochem. Sci.* **20**, 374